

Adaptive tissue segmentation based on MRI

Maxim Nekrashevich, Vladislav Molodtsov,
Dmitry Masnyi, Dmitry Artemasov

May 2022

Abstract

Nowadays, segmentation of the Magnetic resonance imaging (MRI) images is one of the popular subject in medical computer vision. Due to the complex nature of magnetism, different tissues are not always discernible on an MRI image. To address that, there exist many MRI sequences (modalities) which highlight the specific tissues while suppressing others. In this work, we propose a new segmentation technique which uses multiple intermediate MRI slices. We found that this approach outperforms state-of-the-art solutions which use only final reconstructed images. In addition, we present proof of concept of the MRI sequence optimization using backpropagation. Our results are important for MRI industry since the proposed techniques can significantly improve MRI segmentation quality and allow to make more accurate diagnoses when examining patients using MRI.

1 Introduction

1.1 MRI basics

Magnetic resonance imaging (MRI) is a commonly used imaging method, which uses the body's natural magnetic properties to produce detailed images from any part of the body. For image acquisition purposes the hydrogen nucleus is used because of its abundance in water and fat. For the MRI image acquisition, MRI scanners are used. When the body is placed in a MRI scanner the protons' axes all line up in the strong magnetic field. This uniform alignment creates a magnetic vector oriented along the magnetic field of the MRI scanner.

When the energy of a radio frequency (RF) wave is added to the magnetic field of MRI scanner, the magnetic vector of the body deflects. Such deflections depend on the physical properties of a tissue.

In order to make different slices of the body distinguishable, the strength of the magnetic field is altered with a series of gradient electric coils located along the patient's body. Different body tissues will resonate on different frequencies.

When the RF source is switched off, the magnetic vector returns to its resting state, and this causes a target signal (also a radio wave) to be emitted. This signal is detected by receiver coils and then used to create the MR image.

Different tissues relax at different rates when the transmitted RF pulse is switched off. So in order to highlight particular tissues or abnormalities of the body, multiple transmitted RF pulses can be used.[1].

1.2 Literature review

Currently, the MRI-based segmentation is done using images of a certain modalities (e.g., T1, T2, T2*). Modality refers to the form of an imaging [1]. Usually the training process is as follows: a neural network is trained either on image of a particular modality (T1 or T2)[3] or on a stacked images of different modalities (for example T1 and T2) [9, 4]. The image of a particular modality is obtained via algebraic reconstruction technique from a multiple slices acquired during MRI scanning [6].

Broadly speaking, deep learning segmentation methods can be performed with convolutional networks or patch-based classification techniques. The former works on the entire image to make a per-pixel decision in a single run through the trained network, while the latter works on small sections of the image (patches) to predict the likelihood that this patch belong to a particular region (i.e. class) of interest. After this, the patch travels through the network to construct the prediction for the entire image. Convolutional networks take less time to process an image than the patch-based methods when tasked with whole image segmentation or labelling, and present comparable or superior performance in common accuracy metrics.

One of the most popular convolutional neural networks for image segmentation is called U-Net. It was proposed in [12]. U-Net has been used to localise and segment intervertebral discs in MRI images and to segment tissues in CT images such as livers and tumours or various organs in the chest [7]. Another architecture that can be called state-of-art is LiviaNET (3D and convolutional neural network for subcortical brain structure segmentation in MRI). [5] But it has a drawback related to the computational and memory requirements during inference.

1.3 Our contribution

The contribution of this project can be summarized as follows. First, we propose a new segmentation approach. As mentioned above, usually, a neural network is trained only on a single image obtained after reconstruction from multiple MRI slices. Instead of that, we suggest training the neural network on all obtained intermediate slices. We believe that this will allow us improve segmentation quality, since intermediate slices can contain more visual information which is usually lost during final reconstruction.

Second, we present a concept which can improve the MRI segmentation quality by optimizing sequences used to obtain MRI slices. Visual properties of MRI slices obtained strongly depend on the parameters of MRI sequence such as gradients of magnetic field or Radio Frequency (RF) pulses. By tuning MRI sequence, we can make some slices be more distinguishable. Therefore,

the neural network will be able to use such slices in order to perform more accurate segmentation. For MRI sequence optimization, we are going to use backpropagation through Bloch simulator, since all operations in this simulator are differentiable.

The practical relevance of this research is that the proposed segmentation technique and the optimized MRI sequence could significantly improve MRI segmentation quality. As a result, it will help to make more accurate diagnoses when examining patients using MRI.

2 Methods and materials

In this Section, we describe methods and materials used in this work. In Section 2.1, Block simulator used for obtaining MRI slices is described. In Section 2.2, the proposed segmentation techniques using multiple intermediate slices is presented. In Section 2.4, the concept of MRI sequence optimization using backpropagation is given. In Section 2.5, alternative parametrization of MRI sequence is discussed. Finally, in Section 2.3, the summary of finding the best segmentation model is presented.

2.1 Bloch simulator

In this work, we use Bloch simulator [2] for obtaining MRI slices. It takes so-called phantom as an input and produces multiple MRI slices which can be further used to get reconstruction image in some modality.

Each pixel of the phantom is characterized by its proton density (ρ), spin-lattice relaxation time (T1), and spin-spin relaxation time (T2), depending on the tissue class to which it belongs. Each class of tissues has the same physical parameters, i.e. ρ , T1, T2, generated randomly. However, different tissues might have similar values of either ρ , T1 or T2.

In our experiments, we considered phantoms with 5 different classes of tissues including 1 class for background. Therefore, segmentation mask has 5 different classes. An example of the phantom used in our experiments can be found in Figure 1, where ρ map, T1 map, T2 map, and corresponding segmentation mask are depicted.

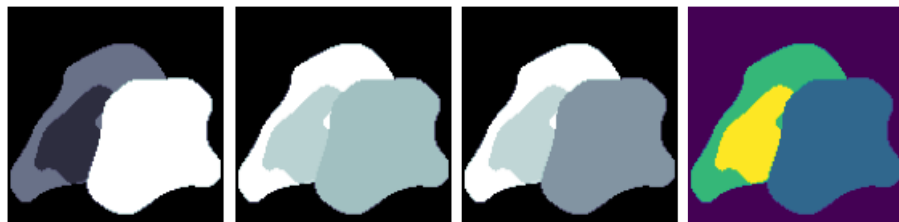


Figure 1: Generated phantom: ρ map, T1 map, T2 map, segmentation mask

Used Bloch simulator sequentially applies predefined RF and field gradients sequences and computes magnetization vectors at each moment of time. Later, MRI slices can be obtained by measuring the total magnetization and applying Algebraic Reconstruction Technique (ART). An example of such slices are presented in Figure 2.

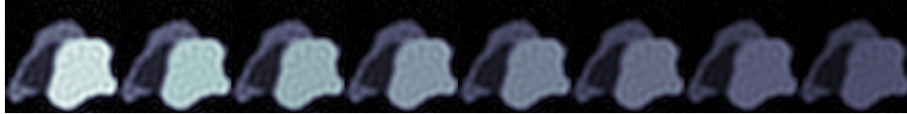


Figure 2: Obtained MRI slices

After we get all intermediate slices, we get reconstructed image in some modality. In our case, initial RF and field gradient sequences were selected in such a way as to obtain the reconstructed image in T2 modality.

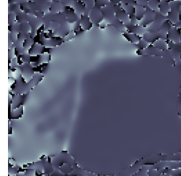


Figure 3: Reconstructed image in T2 modality

Using Bloch simulator, we generated the datasets with different resolutions (128x128, 64x64, 32x32 and 16x16) to test the proposed segmentation technique. As we will mention later, segmentation model can easily handle images with large resolution. However, in Section 2.4, we utilize backpropagation to find the optimal MRI sequence. Thus, we decided to use smaller resolution (16x16) in order to fit all computations into Graphics Random Access Memory (GRAM).

2.2 Proposed segmentation technique

As stated in Section 1.3, state-of-the-art approach in MRI segmentation is to take reconstructed image (see Fig.3) and apply some segmentation model to it. Here, we propose another way which can use more visual information.

Instead of using only one reconstructed image for each phantom, we propose to use intermediate MRI slices (see Fig.2). The motivation behind this idea is as follows. The reconstructed image which is usually used as an input for segmentation model is the representation of the phantom in one particular modality. For instance, in our work, it is T2 modality. However, some tissues can be discernible in the chosen modality. However, it can be well distinguishable in intermediate MRI slices since they are obtained at different time moments after excitation. It brings us to the idea that the usage of these MRI slices can improve the quality of the segmentation model.

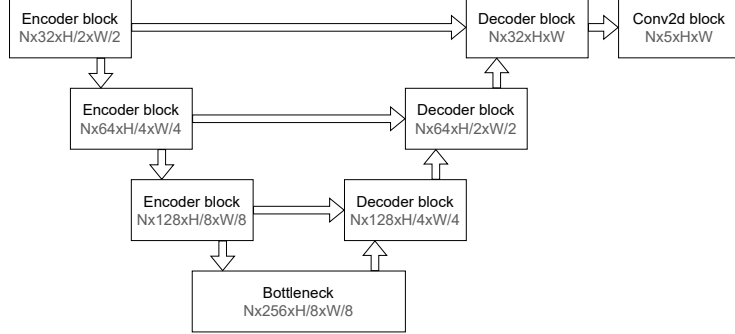


Figure 4: UNet architecture

Thus, in order to prove our hypothesis, we trained neural networks described later in three different scenarios. First, the model took as an input only reconstructed image obtained from multiple slices. Second, it took as an input reconstructed image and the first MRI slice. Third, all MRI slices were used as an input for neural network. For quantitative performance assessment Dice score was chosen since it is common metric for MRI [8]. In addition, we measured mean accuracy and mean Intersection over Union (IoU). Results for all considered scenarios are presented in Section 3.1.

2.3 Segmentation model

For the segmentation task we used UNet model (see Fig. 4) [12]. Encoder block of UNet model consists of layers depicted in Figure 5. For the bottleneck block we used the encoder block but without the max pooling layer at the end. Decoder block consists of the layers depicted in Figure 5. In the decoder block we used dropout layer in order to prevent overfitting of the model. Instance normalisation is used both in encoder and decoder. MRI images could have some artifacts (ambient illuminations) or have different contrasts (within the same batch). Instance normalisation allows to deal with problems described above.

Since Dice score was chosen as a quality metric, we use Dice Loss function, which can be calculated as follows:

$$L_{DICE} = \frac{1}{N_{classes}} \sum_{i=1}^{N_{classes}} 1 - \frac{2 \cdot |P_i \cap Y_i|}{|P_i| + |Y_i|},$$

where P_i denotes pixels predicted to be i -th class, Y_i denotes pixels of i -th class in the mask.

During model tuning, a large number of different parameters was analyzed. The influence of some of them on the performance is depicted in Figure 6. Model training analytics can be accessed by the following links [11, 10]

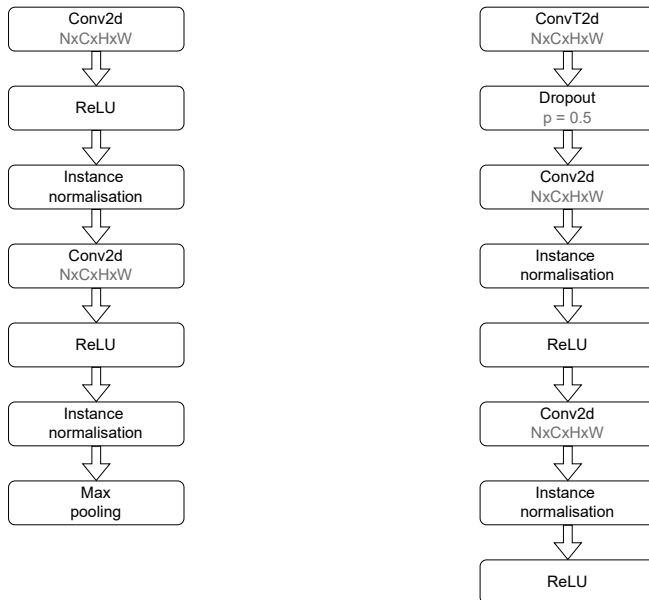


Figure 5: Encoder block's layers (left)
Decoder block's layers(right)

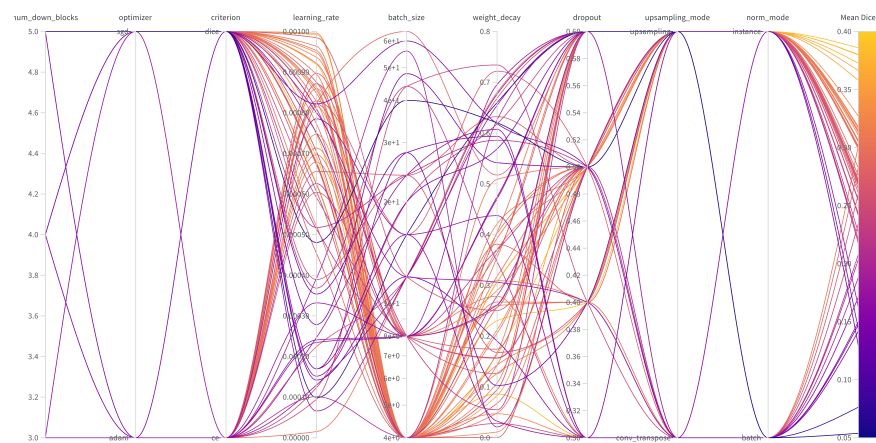


Figure 6: Wandb model parameters optimization sweep

2.4 MRI sequence optimization

Reflections in Section 2.2 lead us to the idea that additional changes of MRI sequence used for obtaining slices could be beneficial, since they can make slices be more distinguishable. Thus, there should be an optimal MRI sequence which will give an opportunity to segment tissues in the most effective way. In this work, we are going to prove the concept that such optimal sequence can be found by backpropagation.

The point is that all operations in Bloch simulator are differentiable. Thus, we can somehow parameterize our MRI sequence, generate MRI slices using such sequence, put obtained slices into the differentiable segmentation model, e.g. neural network which was previously pretrained on MRI slices, compute segmentation loss, backpropagate this loss to our parameters, and update them by e.g. gradient descend. The described pipeline is visualized in Figure 7. The key thing is that this optimized MRI sequence can be further used in real MRI scanners in order to get images with higher quality.

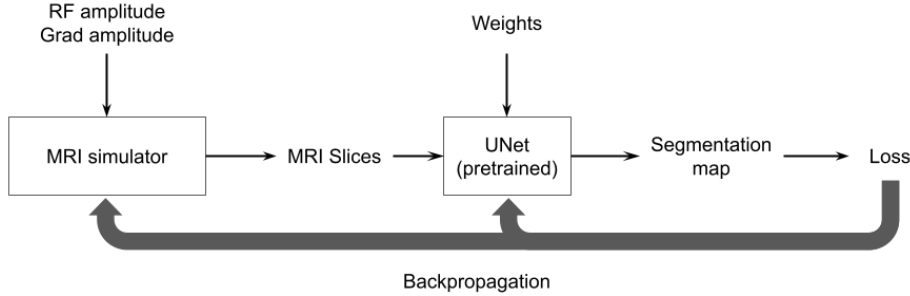


Figure 7: Pipeline of optimizing MRI sequence

The only problem is how to parameterize our MRI sequence. First of all, we utilize the simplest approach when the tunable parameters are the amplitudes of RF pulse and field gradient at each time moment, as depicted in Fig.8b). However, this way of parameterization has some drawbacks which will be discussed and eliminated in Section 2.5.

2.5 Kernels for parametrization

Parameterization of amplitudes at each time step results in huge amount of optimizable parameters which are highly correlated. Moreover, this parametrization somewhat fails to capture the operations of a real-world MRI scanner. And finally, this approach does not allow us to directly optimize the times of events. For instance, in order for a pulse to be shifted in time, the optimizer needs to lower the amplitude of the pulse on one end and increase it on the other.

In this section, we introduce an alternative parameterization of an MRI sequence which can address all these issues. This parameterization treats field gradients and RF pulses as discrete events. Each event is characterized by a

small number of parameters, such as time moment and amplitude. The amplitude can be optimized directly as in the previous case. However, in order to apply backpropagation for optimizing the times of events, we rely on kernels.

We parameterize the RF amplitudes using the triangular kernel:

$$k_{\Delta}(t, t_{pulse}) = 2 \left(1 - \frac{2|t - t_{pulse}|}{w_{pulse}} \right)_{+}$$

Note that the maximum amplitude of the pulse is double that in the original case, which is done in order to preserve the integral of this pulse and thus its total impact on the magnetization.

For the parameterization of gradients we rely on trapezoidal kernel, which is given by the following formula:

$$k_{trapezoid}(t, t_{grad}) = \min(k_{\Delta}(t, t_{grad}), 1)$$

We chose this kernel, as the duration of the gradient is higher than that of the RF pulse and the value at read time is more important than the total contribution.

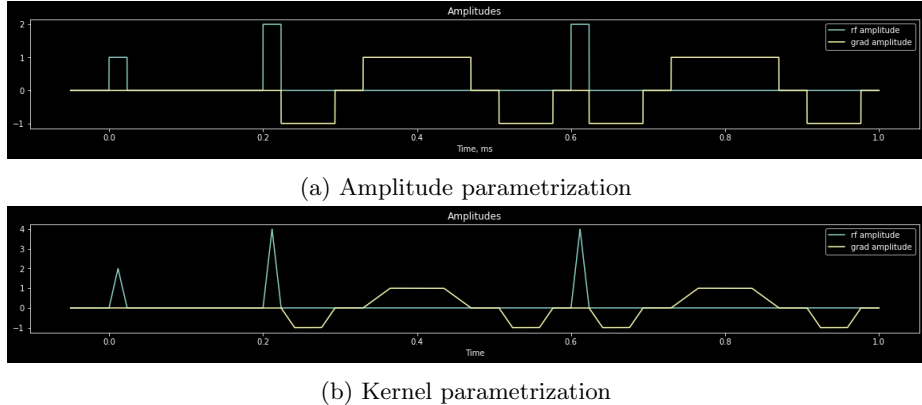


Figure 8: The RF sequence used to obtain two slices for the T2-weighted image. The amplitudes of RF pulses and gradients over time are shown in cyan and yellow respectively. Originally, the amplitudes are constant (see (a)), however in the kernel parametrization, the amplitude follows the shape of the corresponding kernel (see (b)). For the RF pulses, we use the triangular kernel and for the gradients, the trapezoidal one. This results in an explicit dependency on time, thus allowing to propagate the gradients all the way back to the event times.

3 Experimental results

In this Section, we present the obtained results. First, in Section 3.1, we show that the proposed segmentation techniques utilizing multiple intermediate

slices can achieve higher gain compared to the conventional approach used in literature. Second, in Section 3.2, we prove the concept that MRI sequence can be efficiently optimized using backpropagation.

3.1 Proposed segmentation technique

As stated in Section 1.3, existing approach in MRI segmentation is to take reconstructed image (see Fig.3) and apply some segmentation model to it. Here, we compare the state-of-the-art approach with the proposed one.

For that, we took the best model described in Section 2.3 and trained it in three different scenarios. First, we trained the model on only reconstructed images as usually done in literature in order to reproduce state-of-the-art results. Second, we trained the model on both reconstructed images and the first slice, thus, increasing the amount of visual information being used. Finally, the network was trained on all 8 intermediate slices as we propose. Mean Dice metrics as well as mean accuracy and mean IoU for all considered scenarios are reported in Table 1. Note, that all performance metrics were evaluated on a separate validation dataset.

Table 1: Quality metrics for different segmentation techniques

	Reconstructed only (state-of-the-art)	Reconstructed + 1st slice	8 slices
Dice	0.65	0.84	0.92
Accuracy	0.87	0.94	0.96
IoU	0.57	0.77	0.87

Given the obtained results, we can conclude that adding even 1 slice to the reconstructed image can allow the model to get significant gain. At the same time, using all obtained slices outstandingly outperforms all other techniques. These results proved that a direct approach, where the model was trained on multiple intermediate slices, had better performance, because it could use more information that otherwise was lost during the final image reconstruction.

3.2 MRI sequence optimization

For testing MRI sequence optimization, simplified phantom was used since full backpropagation pipeline (see Fig.7) required a lot of GRAM. In Figure 9, ρ map, T1 map, T2 map, and corresponding segmentation mask of the used phantom are depicted. Moreover, we also simplified MRI sequence: the number of RF pulses were reduced from 9 to 3.

Moreover, here, we are interested only in proving the concept that backpropagation can be used for MRI sequence optimization. Our main limitation is that backpropagation for one phantom takes 25 minutes on Nvidia Tesla V100 32Gb. Thus, our goal is just to show that MRI sequence changes in the process of optimization and its changes are beneficial for the final metric. Therefore,

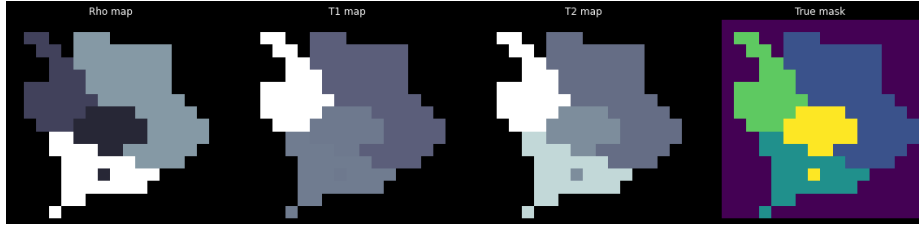


Figure 9: Used phantom: ρ map, T1 map, T2 map, segmentation mask

we train and test our pipeline on the same phantom for simplicity. In addition, first, we have frozen the weights of the UNet model, since we want to emphasize that the metrics improvement is caused by MRI sequence optimization only.

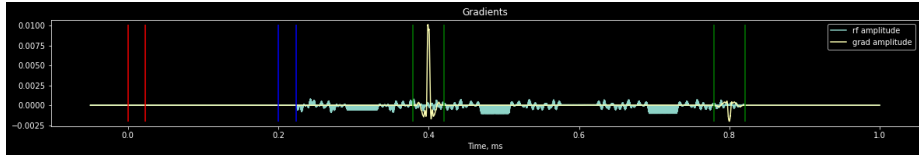


Figure 10: Gradients of tunable parameters at the first iteration

Figure 10 represent the gradients of both RF and field gradient amplitudes after the first backpropagation iteration. Vertical red and blue lines show the positions of RF pulses, while vertical green lines indicate readout intervals. Note, that here, we do not optimize readout moments, but the optimization pipeline has implicit mechanism to adjust them by shifting RF pulses and gradients in time. However, in case of parameterization by amplitudes, it is not practically feasible as discussed in Section 2.5. Moreover, Figure 10 indicates that the position of peaks is quite meaningful. We have non-zero gradients of RF amplitude at the intervals when field gradients are applied. At the same time, non-zero gradients of field amplitude are placed exactly in the center of the readout interval.

From Figure 11, we can observe how our sequences have changed after 30 iterations of Gradient Descend (GD) with learning rate 1. Relatively high learning rate was chosen since the gradients are too tiny.

Figure 12 represents how MRI slices and segmentation by neural network have changed after 30 iterations of backpropagation. As we can see, resulting segmentation mask has been significantly improved. But visually, MRI slices have not changed a lot. However, if we take a look at the difference between initial MRI slice and the resulting one (see Fig.13), we can notice that some meaningful differences have a place to be.

Finally, Figure 14 shows how quality metrics, such as accuracy and Dice, have changed during optimization procedure. As we can observe, the accuracy has increased by 9%, while Dice metric has increased by 2%.

Optionally, we repeated these experiments, but without freezing the weights

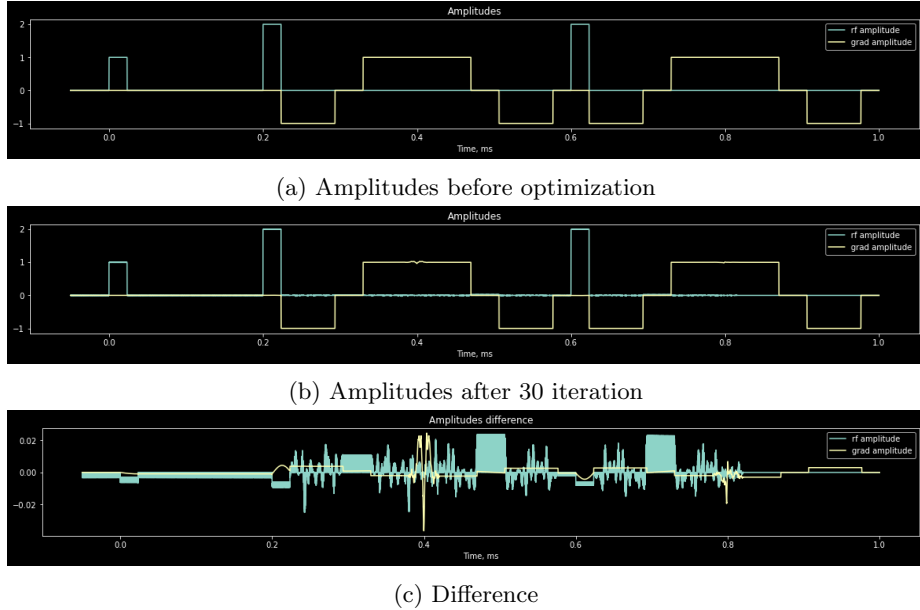


Figure 11: Changes of tunable parameters (model was frozen)

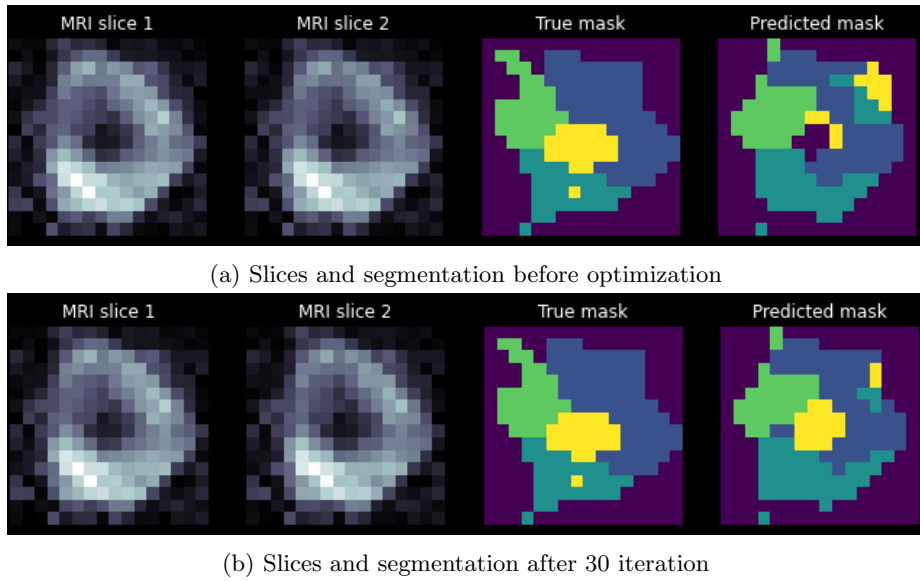


Figure 12: Changes of segmentation (model was frozen)

of the model in order to fine-tune it. In this case, quality metrics have reached much higher values: the accuracy has increased by 20%, while Dice metric has

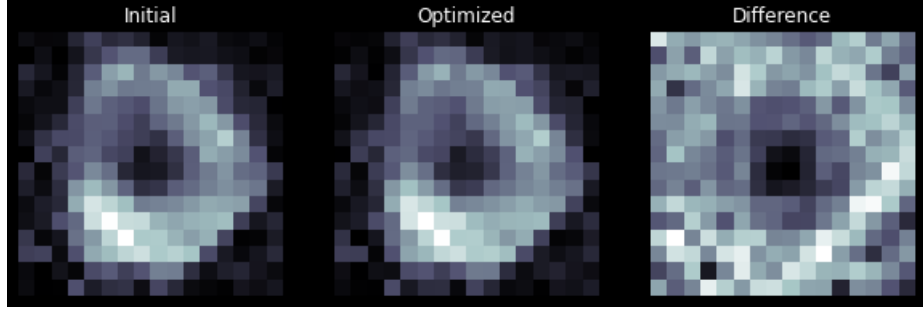


Figure 13: Difference between MRI slices (model was frozen)

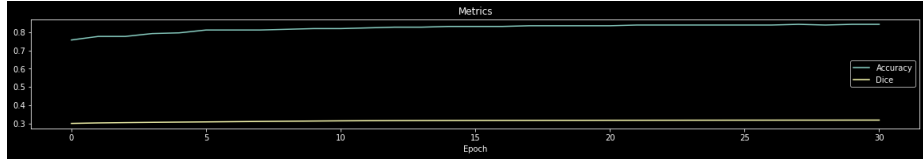


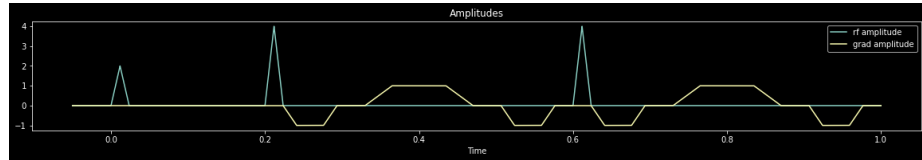
Figure 14: Changes of quality metrics (model was frozen)

increased by 4%. The corresponding figures can be found in Appendix in order to prevent the main text of the report from overloading.

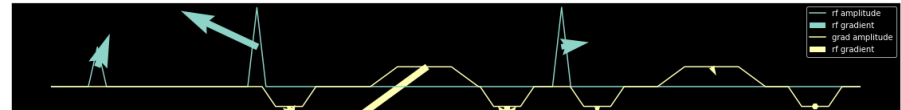
3.3 Kernels for optimization

We conducted the same experiments with kernels. For the parameters, associated with RF pulses, we used GD with learning rate 2e-2. For the parameters, associated with gradients, learning rate 2e-3 was used. Additionally, we performed gradient clipping by 0.05.

Figure 15 indicates how tunable parameters have changed in case of kernel optimization, while Figure 16 shows how MRI slices have changed. Despite we can notice some meaningful changes in both Figures mentioned above, quality metrics depicted in Figure 17 have not significantly improved. A possible reason for this might be that the simulation is too sensitive to even slight changes in such a parametrization. A further reduction of the learning rate might solve this issue, therefore, additional experiments in this field are to be conducted.

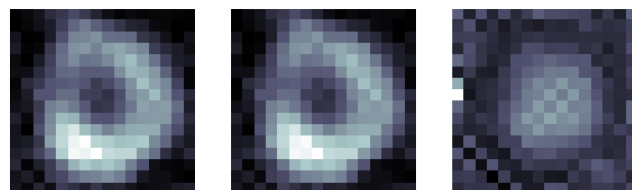


(a) Amplitudes before optimization

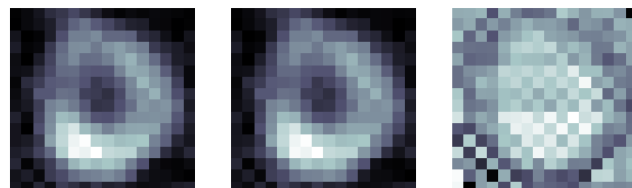


(b) Amplitudes after 10 iteration and corresponding gradients

Figure 15: Changes of tunable parameters by kernel optimization (model was frozen)



(a) Difference in the 1st slice



(b) Difference in the 2nd slice

Figure 16: Changes of slices by kernel optimization (model was frozen)



Figure 17: Changes of quality metrics (model was frozen)

4 Conclusion

In this work, we proposed two ways of improving MRI segmentation quality. The first one is using intermediate MRI slices instead of the final reconstructed image. Our results showed that such a way of defining neural network's input is extremely beneficial, since it allowed the net to use more visual information which is usually lost during reconstruction. Thus, our solution outperforms state-of-the-art approach. The second one is optimizing MRI sequence by back-propagation. We have proven the concept that such optimization is possible and it can lead to improvements of the segmentation quality. The obtained results can be used in MRI industry in order to make the MRI diagnoses even more accurate. Moreover, our techniques can be easily adapted to various other tasks based on MRI e.g., tumor detection, classification, etc.

5 Team members contribution

- Maxim Nekrashevich: leading team, distributing tasks, communicating with TAs and teachers, brainstorming and ideas discussing, implementing MRI sequence optimization and phantom generation, conducting experiments with kernel optimization, building graphs, making report and presentation.
- Vladislav Molodtsov: communicating with TAs and teachers, brainstorming and ideas discussing, simulator's code refactoring, implementing MRI sequence optimization, conducting experiments with MRI sequence optimization, building graphs, making report and presentation.
- Dmitry Masnyi: communicating with TAs and teachers, brainstorming and ideas discussing, simulator's code refactoring, implementing UNet model and a few metrics, making report and presentation.
- Dmitry Artemasov: communicating with TAs and teachers, brainstorming and ideas discussing, implementing UNet architecture, implementing custom dataloader, defining optimal augmentations, model parameters fine-tuning, making report and presentation.

6 Third party code

1. Code for phantoms generation:
https://github.com/yanfengliu/layered_embeddings/blob/master/shapes.py
2. Bloch equations' simulator:
<https://github.com/Airplaneless/bsim> (the repository is private, we attached zip archive with the report)

References

- [1] Abi Berger. “Magnetic resonance imaging”. In: *BMJ* 324.7328 (2002), p. 35. ISSN: 0959-8138. DOI: [10.1136/bmj.324.7328.35](https://doi.org/10.1136/bmj.324.7328.35). eprint: <https://www.bmjjournals.com/content/324/7328/35.full.pdf>. URL: <https://www.bmjjournals.com/content/324/7328/35>.
- [2] Zhipeng Cao et al. “Bloch-based MRI system simulator considering realistic electromagnetic fields for calculation of signal, noise, and specific absorption rate”. In: *Magnetic resonance in medicine* 72.1 (2014), pp. 237–247.
- [3] Yang Ding et al. “Using Deep Convolutional Neural Networks for Neonatal Brain Image Segmentation”. In: *Frontiers in Neuroscience* 14 (2020). ISSN: 1662-453X. DOI: [10.3389/fnins.2020.00207](https://doi.org/10.3389/fnins.2020.00207). URL: <https://www.frontiersin.org/article/10.3389/fnins.2020.00207>.
- [4] Yang Ding et al. “Using deep convolutional neural networks for neonatal brain image segmentation”. In: *Frontiers in neuroscience* 14 (2020), p. 207.
- [5] Jose Dolz, Christian Desrosiers, and Ismail Ben Ayed. “3D fully convolutional networks for subcortical segmentation in MRI: A large-scale study”. In: *NeuroImage* 170 (2018). Segmenting the Brain, pp. 456–470. ISSN: 1053-8119. DOI: <https://doi.org/10.1016/j.neuroimage.2017.04.039>. URL: <https://www.sciencedirect.com/science/article/pii/S1053811917303324>.
- [6] Richard Gordon. “A tutorial on art (algebraic reconstruction techniques)”. In: *IEEE Transactions on Nuclear Science* 21.3 (1974), pp. 78–93. DOI: [10.1109/TNS.1974.6499238](https://doi.org/10.1109/TNS.1974.6499238).
- [7] Jared Hamwood et al. “A deep learning method for automatic segmentation of the bony orbit in MRI and CT images”. In: *Scientific Reports* 11 (July 2021). DOI: [10.1038/s41598-021-93227-3](https://doi.org/10.1038/s41598-021-93227-3).
- [8] Farnaz Hoseini, Asadollah Shahbahrami, and Peyman Bayat. “An efficient implementation of deep convolutional neural networks for MRI segmentation”. In: *Journal of digital imaging* 31.5 (2018), pp. 738–747.
- [9] Ali Işın, Cem Direkoglu, and Melike Şah. “Review of MRI-based brain tumor image segmentation using deep learning methods”. In: *Procedia Computer Science* 102 (2016), pp. 317–324.
- [10] Maxim Nekrashevich, Vladislav Molodtsov, Dmitry Masnyi, Dmitry Artemasov. *Model parameters sweep / Adaptive tissue segmentation based on MRI*. May 2022. URL: <https://wandb.ai/bsim-skt/bsim-sweeps/sweeps/30sppqsh>.
- [11] Maxim Nekrashevich, Vladislav Molodtsov, Dmitry Masnyi, Dmitry Artemasov. *Segmentation model runs / Adaptive tissue segmentation based on MRI*. May 2022. URL: <https://wandb.ai/bsim-skt/bsim>.

- [12] Olaf Ronneberger, Philipp Fischer, and Thomas Brox. “U-Net: Convolutional Networks for Biomedical Image Segmentation”. In: *CoRR* abs/1505.04597 (2015). arXiv: [1505.04597](https://arxiv.org/abs/1505.04597). URL: <http://arxiv.org/abs/1505.04597>.

A Optimization of MRI sequence without model freezing

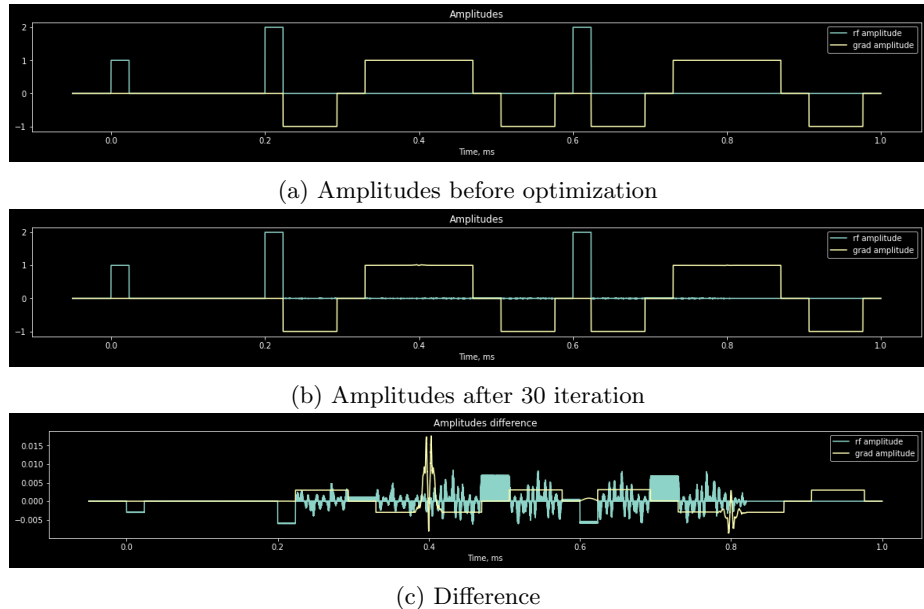
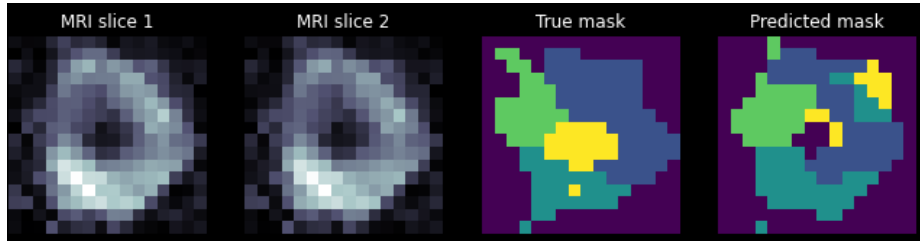
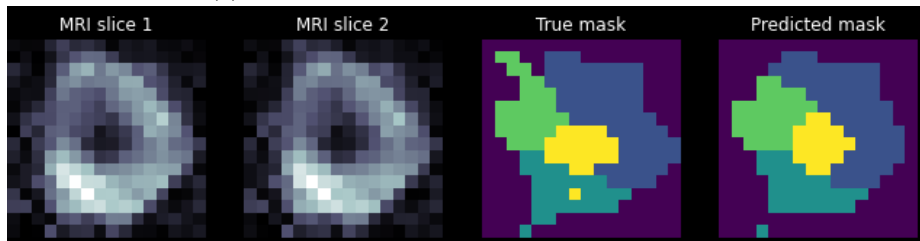


Figure 18: Changes of tunable parameters (model was trained)



(a) Slices and segmentation before optimization



(b) Slices and segmentation after 30 iteration

Figure 19: Changes of segmentation (model was trained)

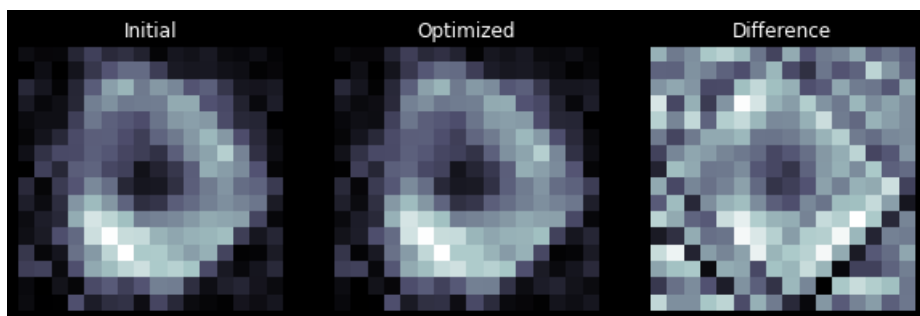


Figure 20: Difference between MRI slices (model was trained)

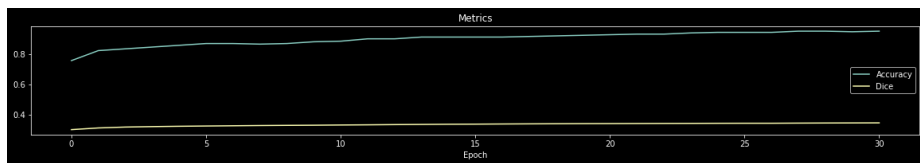


Figure 21: Changes of quality metrics (model was trained)